Light guidance in photonic structures of Morpho butterfly wing scales

Magali Thomé, Elodie Richalot, Serge Berthier

Light guidance in photonic structures of Morpho butterfly wing scales

MAGALI THOME,[1,*] ELODIE RICHALOT,[2,*] AND SERGE BERTHIER[3,1]

[1] *Institut des Nanosciences de Paris, UMR CNRS 7588, Sorbonne Université, France*
[2]*ESYCOM Laboratory (UMR 9007),Univ Gustave Eiffel, CNRS, F-77454 Marne-la-Vallée Cedex 2, France*
[3]*Université de Paris, France*

Abstract: In this paper we investigate the impact of the periodicity along three orthogonal axes of the blue wing scales of *Morpho* butterflies, whereas most of previous studies modeled the scale structure only considering one or two photonic crystal dimensions. Moreover, the previous optical studies of these scales focused on the light reflected by the wing whereas we investigate the light propagation along the lamellae, this direction corresponding to the third dimension of the photonic crystal structure. Simulation results obtained using the finite element method are compared with measurements and/or literature. These calculations, performed for different scale models and orientations, show that a significant part of the non-reflected light, essentially red and infrared, is guided by the lamellae towards the base of the scales where it can be more easily absorbed and the heat more quickly transferred to the hemolymph. This new phenomenon could contribute to the thermal balance of the insect and further illustrates the multifunctionality of the wings of Lepidoptera.

1. Introduction

Some species of *Morpho* butterflies are famous for the metallic blue color seen on the dorsal side of their wings. For example, we can mention the males of *Morpho menelaus* or *Morpho rhetenor* species (Fig. 1). Thanks to the use of electron microscopy in biology from the 1940s [1], we now know that this specific color results from optical interactions between illuminating light and the periodic sub-structures of wings (which are scales, ridges and lamellae shown in Figure 2) [2-8]. Interference and diffraction phenomena, respectively generated by light interactions with a stack of nanometric lamellae and a grating of micrometric ridges, result in the reflection of blue wavelength light. Thus, the blue color does not result from blue pigment absorption, but is mainly due to the wing geometry.

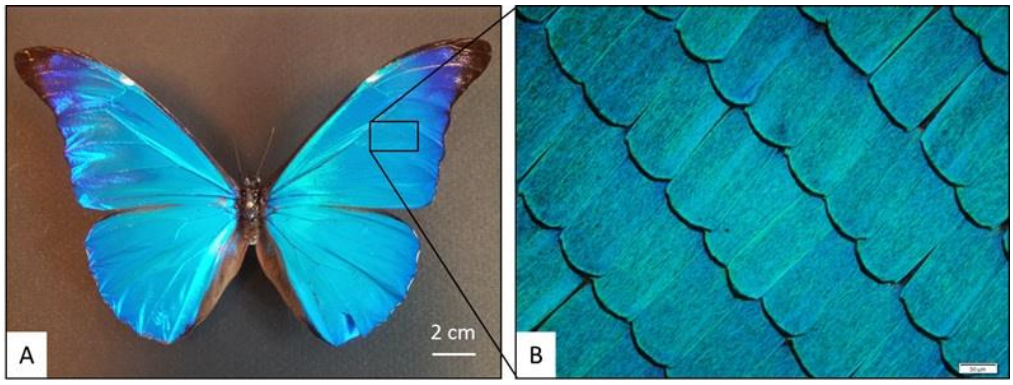

Fig. 1. Dorsal side of a *Morpho rhetenor* male: A) Macroscopic view; B) Magnified view (using an optical microscope) revealing the scales which cover each wing.

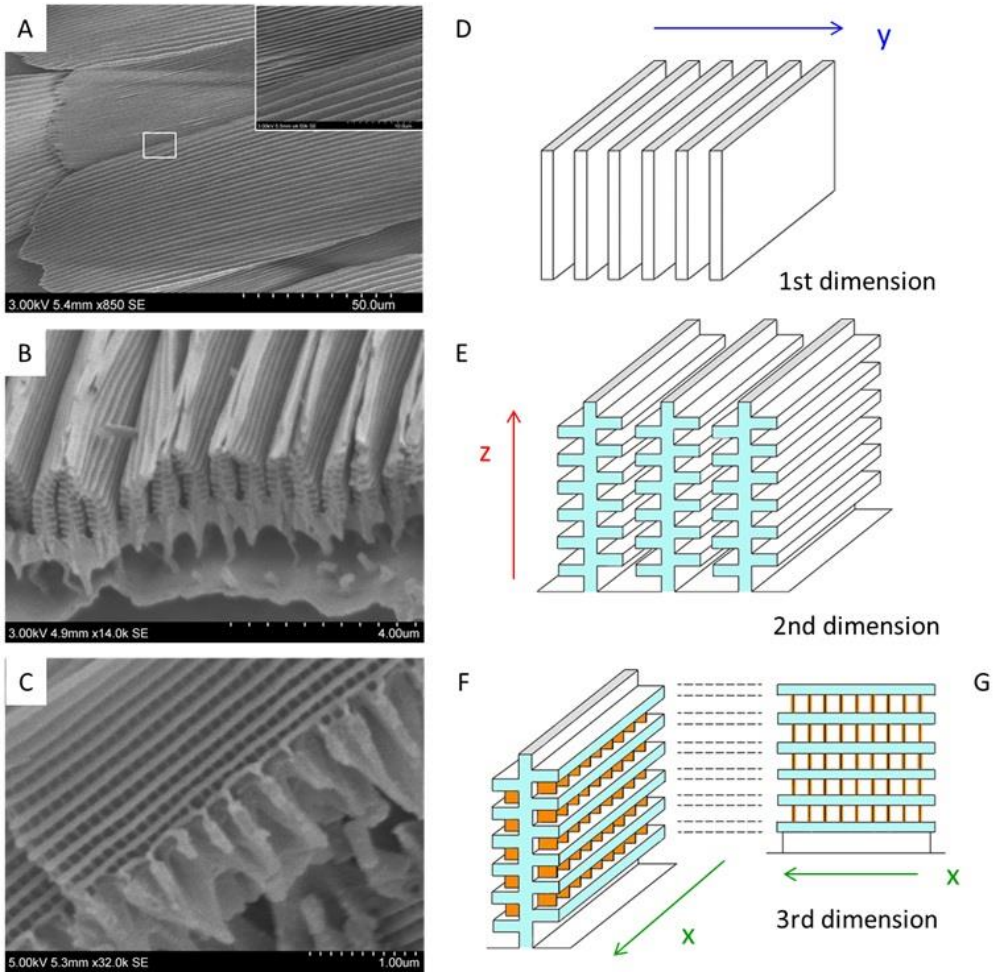

Fig. 2. Scanning Electron Microscopy (SEM) images and schematic representations of the three periodicities of a *Morphidae* blue scale: the ridges lattice (A, D), the lamellae multilayer (B, E), and the membranes between the lamellae called "microribs" (C, F, G). The periodic structure consists of an alternation of air and a chitin-proteins complex. The periodic alternation of the two different refractive indices (air and chitin-proteins complex) is present at different length scales and for different directions: the y direction for the ridges grating (in grey), the z direction for the lamellae multilayer (in blue) and the x direction for the microribs (in orange). Figure 2.G gives a schematic representation of the SEM image in Figure 2.C: it shows a side view of a ridge and emphasizes the presence of microribs.

Other contributions to this blue color reflection have also been highlighted in recent years, using modeling approaches or experimental studies. In particular, the controlled disorder of the wing geometry, including size variations over a scale as well as scales orientation disorder, has been shown to broaden the blue reflection peak [9, 10]. Another example concerns the presence of melanin inside the sub-micrometric structure which seems to reinforce the blue color saturation [11]. Besides these theoretical studies on the origin(s) of this blue, researchers have tried to reproduce this optical effect by making structures more or less similar to real butterfly wing template [4, 12-21]. Thus to obtain inverse or direct replicas of the wing geometry,

different techniques have been used : we can mention a direct writing by electron beam lithography [12] or using a Focused Ion Beam (FIB) [13], the Atomic Layer Deposition method [14, 15], precursors infiltration methods [16-19], and sol-gel deposition [20].

Most of the studies on *Morpho* butterflies focus on the blue color of some males, in other words the light reflected by the dorsal side of their wings. In this paper, we propose to change the traditional viewing angle by studying the light propagation along the lamellae towards the wing membrane. Our interest for this direction has been aroused regarding our *Morpho* blue wing replicas obtained using sol-gel deposition in a previous work [21]. Indeed, these inverse replicas highlight the quasi-perfect lattice formed by the microribs, the smallest scale sub-structures (shown in orange in Figure 2.F). These microribs are located between lamellae, orthogonally to the lamellae length, and regularly spaced along them. We have thus decided to investigate, using finite element calculations, the transmitted light in this later direction corresponding to the third periodicity direction of the photonic crystal formed by the blue wing scale.

In the first part of this paper, we describe the chosen *Morpho* wing structure. A second part is then dedicated to the modeling method and the evaluated parameters, and finally in a third part, our results are presented in graphical form and discussed. We present in particular the reflectance of the wing (ratio of the reflected radiant flux to the incident one) and its transmittance (considering the transmitted radiant flux) in the lamellae direction.

2. The Morpho blue wing: a natural 3D photonic structure

The studied *Morpho* wing structure we chose is a *Morpho rhetenor* one (Fig. 1). This blue wing is multiscaled, that is to say composed of different sub-structures at different length ranges: the centimeter, micrometer and nanometer ones (Fig. 2). First of all, the wing (about 5 cm long) is covered with scales (100 µm long and 50 µm wide) arranged like roof tiles (Figs. 1.B and 2.A). There are two different types of scales: transparent cover scales and blue ground scales, but the cover scales of *Morpho rhetenor* are atrophied. In this particular case, the macroscopic color of *Morpho* wing is mainly due to ground scales. It explains our species choice: the *Morpho rhetenor* wing structure is easier to model as only one scale type is considered. When looking at these ground scales, it appears that each one is covered with a lattice of parallel ridges (600 nm apart), each ridge being provided by a stack of 11-12 lamellae (about 50 nm thick) (Fig. 2.B). The cross-section of a ridge presents ~~of~~ a Christmas tree shape, schematically shown in blue in Figure 2.E. Optically behaving as a multilayer (of 100 nm period), the stack of lamellae selects a blue color by interferences, whereas the lattice of ridges scatters this blue light by diffraction [2,3].

Due to the periodic nature of its sub-structures and the associated control of light, a *Morpho* blue wing can be regarded as a photonic crystal. It can be presented as a one-dimensional, two-dimensional or three-dimensional photonic crystal, as we consider or not all the periodic sub-structures. This natural photonic crystal is viewed as a two-dimensional one while considering the propagation within the plane formed by the periodicity axis of the ridge grating (y-direction in Figure 2.D) and the normal to lamellae multilayer (z-direction in Figure 2.E). The blue scale is viewed as a 3D photonic crystal when also considering the presence of microribs that are small membranes between the lamellae (Scanning Electron Microcopy (SEM) image in Figure 2.C or schematically in orange in Figures 2.F and 2.G). They are arranged like a quasi-perfect lattice of 30 nm thick membranes periodically separated with air. Depending on SEM images, the measured spacing between adjacent microribs is comprised between 60 nm and 105 nm.

Thus, the periodic arrangement of microribs forms a third periodicity of the wing scale geometry whose direction corresponds to the third space dimension (x direction in Figure 2.F). These periodic microribs complete the description of our natural 3D photonic structure presenting three orthogonal periodicity directions at three different length scales.

3. Modeling: unit cell, indicators and method

The detailed structure of the studied wing scale being now presented, we move to the 3D electromagnetic modeling using the finite element approach to determine its electromagnetic behavior. The use of this electromagnetic modeling method to determine the optical response of the *Morpho* scale has already been validated in a previous article published in 2013 by Mejdoubi et al. (for a 3D model) [22] and in the work of Siddique et al. in 2013 (for a 2D model) [23]. Several other methods have also been used and presented in literature, as the Finite-Difference Time-Domain method (FDTD) [24-27], the Rigorous Coupled-Wave Analysis (RCWA) [28-29], and a modal method similar to the RCWA [30]. Most of these authors used 2D models and therefore could not take into account the presence of microribs. For this purpose, a 3D model is necessary and a 3D finite element approach allows its accurate simulation.

As the finite element method can only handle small volumes in terms of wavelength, the periodic structure of the studied scale is modeled by infinitely repeating a unit cell along two space directions (namely x and y directions) (Fig. 3A), thanks to specific boundary conditions imposed on the vertical faces of the studied unit cell: periodic boundary conditions emulate the infinite periodicity along x and y directions. Other boundary conditions, namely Perfectly Matched Layers (PML), are used at the top and bottom faces (orthogonal to z-axis) to model free-space propagation of the incident wave in the (-z) direction.

The finite element method appears very well suited to model the electromagnetic properties of a *Morpho* blue wing as it permits a precise description of the 3D scale geometry. However, the arrangement of scales on the wing, and the structural disorder between them, cannot be reproduced by this way because of the large area that would have to be modeled. We only can model an infinite periodic scale and consider it as representative of the whole wing.

3.2 Unit cells

Based on the work of Mejdoubi et al. [22] previously performed in our team, the simulated geometry, composed of two ridges, has been improved to more precisely model the real scale structure deduced from several photographs. The thickness of the lamellae was slightly reduced and we added the 160 nm thick scale membrane (Fig. 3.A), the 30 nm thick microribs (Fig. 3.B) and the holes present at the bottom of the ridges (200 nm diameter) (Fig. 3.C).

Four different versions of this new cell have been studied. The two first ones called version 1 and version 2 take into account the presence of microribs spaced respectively by 60 nm and 105 nm along x-axis (Fig. 3.B). They correspond to the more realistic geometries. To better understand the effect of the microribs, we have also extracted the optical properties of a model without microribs called version 3 (Figure 4.A) and a model with microribs of infinite thickness called version 4 (Fig. 4.B, the space between lamellae being filled in this case). In Section 4, the simulation results associated with these 4 models will be compared.

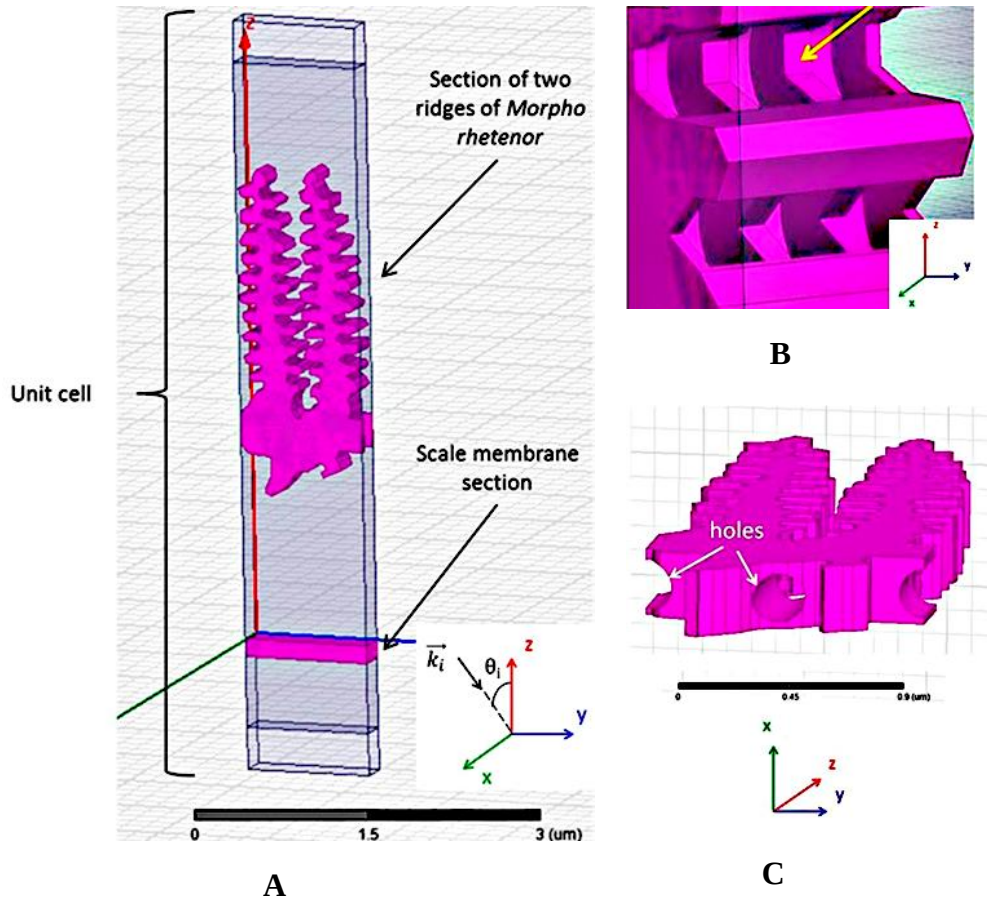

Fig. 3. A) Studied unit cell composed of two ridges of a *Morpho rhetenor* scale and considering the presence of the scale membrane (pointed by a black arrow). The incidence direction of illuminating plane wave in xz plane is indicated by θ_i angle with respect to z-axis. B) Details of the 30 nm thick microribs (pointed by a yellow arrow) located between lamellae and spaced by 60 nm apart (for unit cell version 1). C) Holes present at the bottom of the ridges (200 nm diameter).

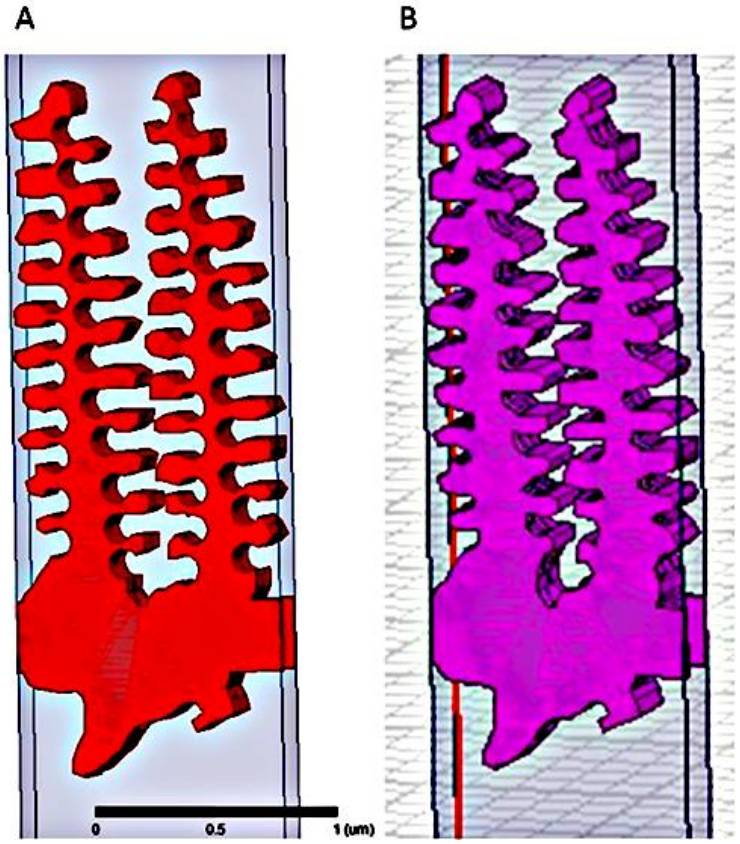

Fig. 4. Two of the unit cells versions: A) version 3 : the two ridges geometry is drawn without microribs; B) version 4 : the microribs between lamellae are characterized by an infinite thickness. It results in a general thickening of ridges and lamellae.

3.3 Optical properties

We investigate a frequency range from 750 THz (wavelength of 400 nm) to 350 THz (or 857 nm). Our model considers the dispersion of the material optical properties versus wavelength, so the complex refractive index can be written $\tilde{n}(\lambda) = n(\lambda) + ik(\lambda)$. Several refractive index values are available in literature: the constant n = 1.56 is often mentioned for works on optical properties of insects [3, 31, 32] and curves of real index dispersion have been presented over the visible wavelength range [33-37]. In these last papers, the n values are comprised between 1.53 and 2, and the k values of the imaginary part are between 0.02 and 0.14. In this work, we have chosen to measure the cuticle (wing material) index of a *Morpho* species, according to a new approach in which measurements are made on the wing membrane. We assume that the material of the wing membrane is the same as the ridges one (composed of the same melanin-chitin-proteins complex). In this calculation, the refractive index is determined by fitting the measured reflectance and transmittance of the wing membrane (see supplementary materials). The dispersive properties of the obtained complex refractive index are taken into account in simulations.

4. Results and discussion

To show the relevancy of our unit cell model, we calculate the reflectance R versus wavelength for each unit cell version presented above (Figs. 3 and 4). As the incident light is not polarized in measurements, simulations are performed while considering successively, for the incident field propagating along xz plane, the two electromagnetic polarizations: the Transverse Magnetic (TM) polarization with electric field tangential to the incidence plane, and the Transverse Electric (TE) polarization with electric field normal to xz incidence plane. The reflectance is then obtained for each polarization from incident and reflected Poynting vector flows through surfaces placed above the sample and normal to the incidence and reflection directions. The total reflectance R presented in this paper is the arithmetic mean of the ones associated to TM and TE incident polarizations:

$$R(\lambda) = \frac{R_{TM}(\lambda)+R_{TE}(\lambda)}{2} \quad (1)$$

It has to be noticed that, as conversion between TE and TM polarizations could occur, the reflected Poynting vector flow may contain a polarization conversion contribution. We have chosen not to distinguish both contributions to use the same indicator as in measurement.

In order to check our proposed wing model is suited to study the optical behavior of real wing, the simulated averaged reflectances are compared with measurements on a natural *Morpho rhetenor* wing. Experiments have been performed using the spectrophotometer Cary 5000 equipped with an integrating sphere and using a normally incident light beam illuminating a wing surface of 1 cm^2. In order to consider both incident polarizations, reflectances are deduced from intensity measurements obtained for two orthogonal positions of the wing sample. The experimental averaged reflectance R presented in Figure 5.A and compared to simulation results corresponds to the arithmetic mean of the reflectances obtained for both sample positions..

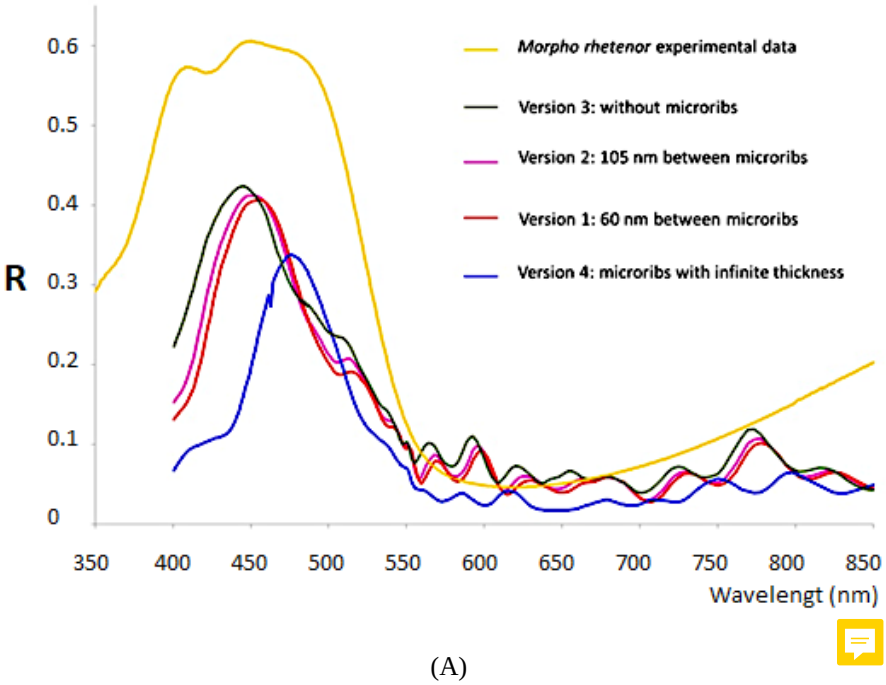

(A)

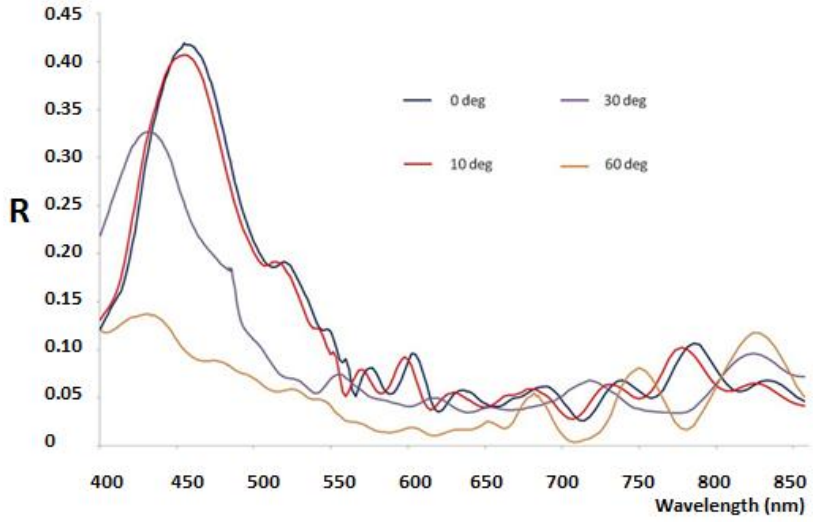

(B)

Fig. 5. A) Comparison between measured (in yellow) and simulated reflectances of a *Morpho rhetenor* wing. The results obtained for the 4 presented versions of the simulated unit cell are shown: version 1 in red, version 2 in pink, version 3 in green, version 4 in blue. The incident plane wave used in modeling has an incidence angle θ_i in the xz plane of 10° to correspond to experimental conditions. B) Comparison of simulated reflectances of the version 1 model (with microribs spaced apart by 60 nm) for different incidence angles of the illuminating plane wave in xz plane: the typical iridescence of the *Morpho* wing is observed via the shift of the maximum reflectance wavelength when the incidence angle increases.

We can see in Figure 5.A that the wavelength corresponding to the maximum of reflection (450 nm) is very similar in experiments and simulations when considering unit cell models version 1 (microribs spaced by 60 nm), version 2 (microribs spaced by 105 nm), and version 3 (without microribs). A significant difference is only visible with version 4 (infinite microribs) response, for which the maximum reflection wavelength is higher. This shift to longer wavelengths can be explained using a simple multilayer model of alternatively air and chitin-proteins complex films. The associated interferential effect leads to an increase of the maximum reflection wavelength with an increase the thickness of higher refractive index films [38]. Even if the simple model used in our simulations, reduced to a small cell infinitely repeated along two axes, cannot totally represent the complexity of the real wing, the similarities between simulated and measured reflectances show the suitability of our model for studying the electromagnetic properties of the *Morpho* wing.

To verify that our model can reproduce the iridescence phenomenon observed with blue *Morpho* wings, simulations have been performed by varying the angle of incidence of the illuminating plane wave in xz plane (Figure 5.B). As expected and observed with *Morpho* butterflies, the optical response shows a shift of the main reflection peak to shorter wavelengths when the incidence angle increases: thus the observed color turns from blue to purple. This wavelength shift is associated to a decrease of the peak reflectance value; this decrease of color intensity is also observed with natural wings.

It is to be mentioned that, even if the reflectance profiles are quite similar at 0° and 10° of incidence, comparison with measurement results are performed in Figure 5.A with a 10° incidence angle as it is closer to experimental conditions. In our measurement, using a Cary 5000 spectrophotometer equipped with a microspot tool and an integrating sphere, the incident light arrives perpendicularly to the wing laying on the ventral side membrane. Nevertheless, the scales and the lamellae are not parallel to the wing membrane. The ridges are tilted from the scale membrane by about 3° whereas the scales are fixed on the wing membrane with an inclination angle of about 7° [38], resulting in a total tilt of 10° between ridges and the wing membrane in the xz plane (Figure 6.A). Therefore, the incident plane wave used in our simulations has a 10° angle of incidence in xz plane, unless otherwise noted.

In addition to the reflectance, the power transmitted in the lamellae direction has also been extracted from simulation results. This propagation direction, indicated by x direction in Figures 3, 6 and 7, is of particular interest as it points towards the wing membrane. The dorsal wing membrane is connected to scales through pedicels pointed in Figures 6.A, C and D by red arrows. Thanks to simulations, we can thus quantify light power propagating in the lamellae direction towards the wing membrane.

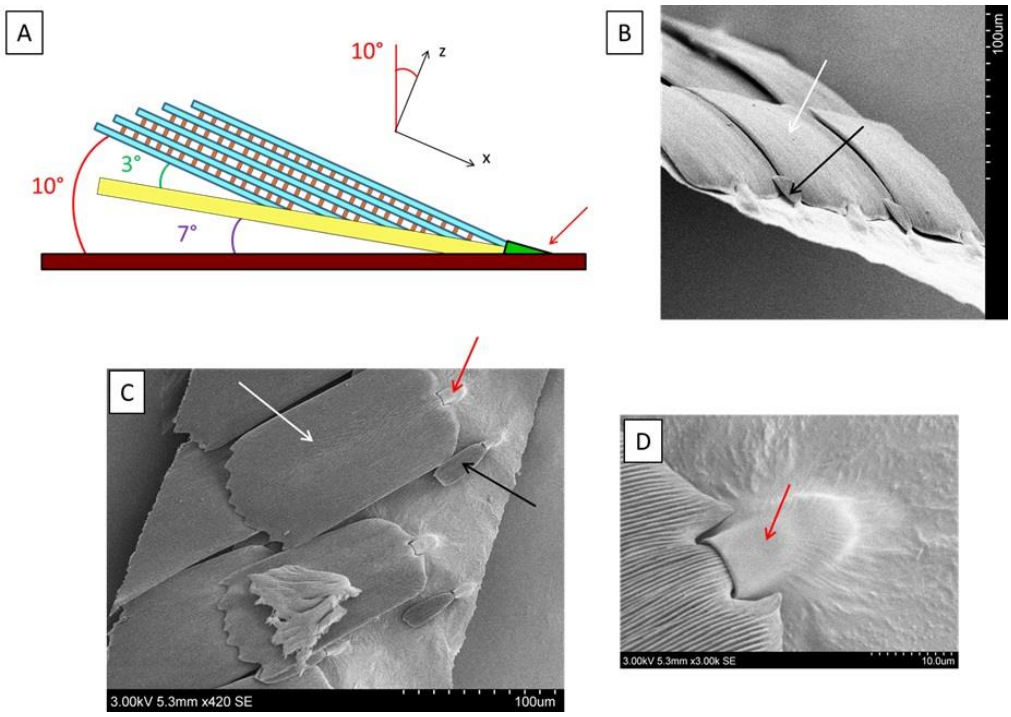

Fig. 6. A) Schematic drawing of a longitudinal section of a *Morpho* ground scale to show the different slopes of the scale structure on the wing membrane: in brown the wing membrane; in yellow the scale membrane; in blue the lamellae of one ridge; and in orange the microribs. The two last colors and the mentioned directions are the same as in Figure 2. E), F) and G) Magnifications of scales of *Morpho rhetenor* blue wing: the ridge lattices of ground scales are pointed by white arrows, the atrophied cover scales are pointed by black arrows and the pedicels which link scales with wing membrane are pointed by red arrows in the 4 pictures.

A

$$T_{TM} = \frac{P_{\text{with scale model (TM)}}}{P_{\text{without scale (TM)}}}$$

$$T_{TM} = \frac{Re\left(\int_S \mathbf{\Pi}_{\text{with scale model (TM)}} \cdot d\mathbf{S}\right)}{Re\left(\int_S \mathbf{\Pi}_{\text{without scale (TM)}} \cdot d\mathbf{S}\right)}$$

$$T = \frac{T_{TM} + T_{TE}}{2}$$

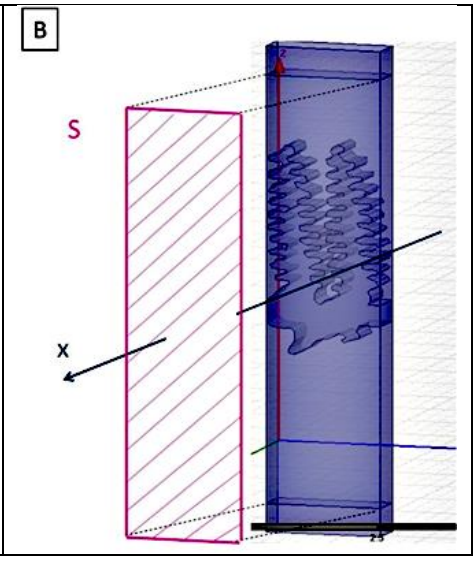

Fig. 7. A) Transmittance T mathematical formulae used in this paper; B) Schematic drawing of the integration surface S of Poynting vector $\vec{\Pi}$ flow.

This transmitted power is evaluated as a transmittance T which is the ratio between the power transmitted through the lateral cell surface S in the presence of the scale model (Figure 7.B) and the power transmitted through the same surface in free-space (in the absence of the scale in the simulated volume). Both powers are calculated as the flow of Poynting vector through S. The surface S does not exactly correspond to the lateral surface of the unit cell as it ends before the scale membrane to only consider the transmission through both ridges. Both polarizations are considered for the incident plane wave and the arithmetic mean of TE and TM transmittances is then calculated (Figure 7.A). The simulated averaged transmittances T are presented in Figures 8 and 9.

Firstly, Figure 8 shows the transmittances versus wavelength for different incidence angles in xz plane (10°, 30°, 60°, and 70°) when considering the version 1 model (the most realistic one). We observe a strong transmittance increase from shorter wavelengths to higher ones, with values between 5% and 15% at 400 nm against 30% to 60% at 800 nm. The near-infrared wavelengths are thus better guided along the lamellae to the wing membrane than the visible ones.

Butterflies are heliothermal organisms, that is, they get most of their energy from sunlight. The latter is either directly absorbed by the wings and transmitted to the muscles via the hemolymphatic network which crosses them (dark butterflies), or directly concentrated on the thorax by the wings playing the role of concentrator (light butterflies). *Morphos* is a special case, with males of almost half of the species reflecting a very large part of the violet, blue and green radiations, that is to say the most energetic part of the solar spectrum. Females, with the exception of those of the genus *Morphos*, are essentially pigmentary coloured and therefore do not have this problem [39-41].

We can thus presume that collecting infrared light is helpful for butterfly to warm up. The light heat could be transmitted from the membrane to its lymphatic lattice. This precise guiding seems to participate to the energy balance of the *Morpho* butterfly.

We can also note that the highest transmittances are obtained whatever the wavelength for the 10° angle of incidence. Thus, for this angle corresponding to an incidence normal to the wing membrane (Figure 6.A), the membrane receives the maximum of light power.

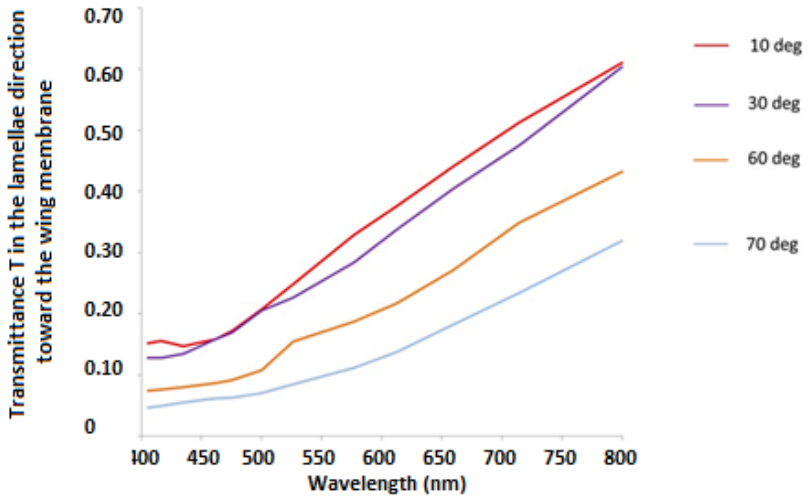

Fig. 8. Transmittances T versus wavelength for the version 1 model (the most realistic one) and for different incidence angles of the illuminating plane wave in xz plane.

Figure 9 shows the transmittances versus wavelength for a 10° degree incidence angle and for the four different versions of the scale model. Little difference is observed between the results obtained with the first three models, despite a slight decrease of the transmission with the insertion of microribs. To observe a more significant difference of the transmittance values, the quantity of matter between the lamellae has to be more important, as with microribs of infinite thickness (version 4); indeed, light is worse guided with thicker ridges. It means that the presence of cavities between microribs improves light flow towards wing membrane, in particular in the near-infrared range. Due to their small thickness in terms of wavelength (30nm), the influence of microribs on optical properties is weak: reflection and transmission properties observed for the three models with thin ridges (versions 1, 2 and 3) are very similar.

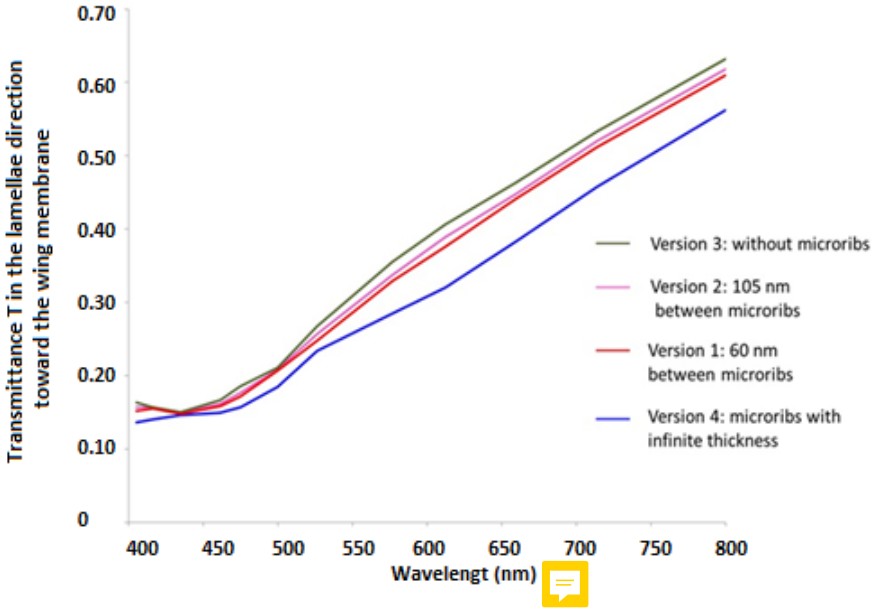

Fig. 9. Transmittances T versus wavelength for an incidence angle of 10° and for different scale models.

The comparison of electric field amplitude cartographies associated with the models version 1 (microribs spaced by 60 nm) and version 3 (without microribs) also shows the weak influence of the presence of microribs, regardless of the polarization TM or TE. Figure 10 presents this comparison for a TM polarized incident plane wave; very similar results are obtained for TE polarization. Whereas the thinness of ridges and lamellae facilitates near-infrared light flow towards the wing membrane, and consequently butterfly warming, the role of microribs doesn't seem to concern the optical behavior but is maybe only mechanical, to keep the lamellae parallel to each other despite the thinness of their junction to ridges.

These observations are also consistent with literature, in particular regarding the impact of microribs on the reflectance. To our knowledge, Lee and al. [24] are the only ones who have studied (using FDTD simulations) a 3D model of a *Morpho rhetenor* wing considering microribs. Their study, that only concerns light scattering by the wing and not its transmission to the membrane as in the present paper, does not show a particular photonic role of these small structures. Regarding the transmitted light to the wing membrane, we have shown that the thinness of ridges and lamellae associated to microribs improves light guiding by lamellae structure.

5. Conclusion

Using simulations and measurements, we have studied in this paper the optical behavior of a *Morpho rhetenor* wing in visible and near-infrared ranges. This study has focused on a new direction of propagation, namely the third dimension of the natural photonic crystal formed by blue wing scales. We have shown that the light is transmitted towards the wing membrane, in particular in the near-infrared range; this phenomenon probably participates to butterfly heating. The architecture of the lamellae lattice appears to favor this guiding of light. The presence of microribs, whose role could be mechanical to keep the thin lamellae parallel to each other despite wing movements, permits ridges and lamellae to be thinner and, as a consequence, improves the near-infrared light propagation towards the wing membrane.

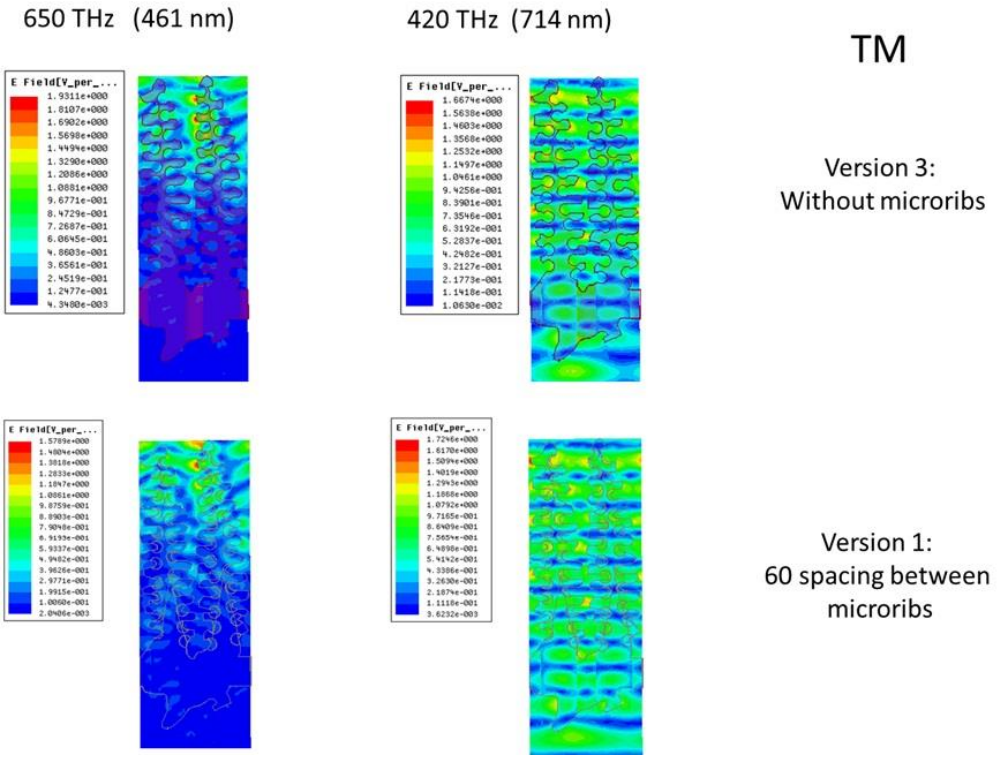

Fig. 10. Electric field amplitude cartographies associated with version 3 and version 1 unit cells for a TM incident plane wave of 10° incidence angle. Whether the microribs are present or not, light easier propagates through the structure at higher wavelength (714nm) than at shorter one (461nm).

SUPPLEMENTARY MATERIALS

Alary membrane.

The wing consists of a double membrane, both developed independently and united at the final formation stage of the wings. The membranes are stretched over a network of tracheae that provide lymphatic circulation. These tracheae are connected by a very dense network of tracheoles on which the different types of scales are implanted. Thus, each scale is directly connected to the network of veins [42].

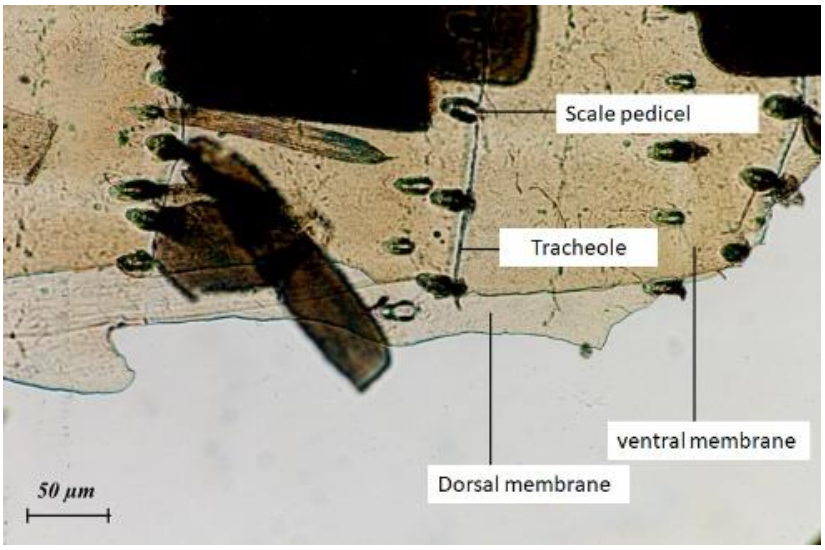

Figure S-1. *Morpho menelaus* alary membrane. Most of the scales were removed on both sides. One can distinguish the two membranes of the wing, and on the ventral membrane, the scales pedicels joined by a thin tracheole.

Finite element method

The finite element method involves the exact resolution of Maxwell equations in the frequency or time domains. In this work, we use the commercial software ANSYS HFSS based on the finite element method applied in the frequency domain. Any complex shape can be drawn and the material properties are described through their complex permittivity and permeability. From simulation results of the considered model, we have extracted the reflected electric field $\vec{E}$, the amplitude reflection coefficient r as well as the reflectance R according to:

$$r = \frac{E_r}{E_0} \qquad \text{(S-1)}$$

$$R = |r|^2 = \frac{\Phi_r}{\Phi_0} \qquad \text{(S-2)}$$

$$\Phi = Re(\int_S \vec{\Pi}.d\vec{S}) = Re(\int_S \frac{\vec{E}\wedge\vec{B}}{\mu_0}.\overrightarrow{dS}) \qquad \text{(S-3)}$$

Where E_r and E_0 correspond respectively to the amplitudes of the reflected electric field and of the incident electric field, Φ_r and Φ_0 correspond to the reflected and incident flows of the Poynting vector $\vec{\Pi}$ through the surface S situated above the simulated scale, μ_0 is the vacuum permittivity.

Refractive index determination

To measure the n and k values, we first remove scales from both sides of a *Morpho menelaus* wing using a razor blade (Fig. S-2.A). The wing membrane appears and we measure the reflectance R (ratio of the reflected radiant flux to the incident one) and the transmittance T (considering the transmitted radiant flux) of this membrane. To do this, we use a Cary 5000 spectrophotometer equipped with an integrating sphere. Due to the small sample size in this case, a microspot tool is used to generate a 1mm diameter illuminating spot. To extract the complex refractive index, the measured reflectance and transmittance are then fitted to a simplified model of the membrane (one 860 nm thick layer of infinite lateral dimensions) through the use of a commercial multilayer modeling software called "Filmwizard" from CSI [43]. This 860 nm thickness of the membrane model corresponds to the average value of thickness measurements performed on SEM cross-section images of the real membrane shown in Figure S-2.A. The initial refractive index of the membrane used to initialize the optimization process, chosen from the paper of Vukusic et al. [32], is equal to the constant complex value 1.56 + i 0.06. Finally, through the fitting process, the software calculates n and k values of the wing membrane for wavelengths from 250 nm to 800 nm. The obtained values are presented in Figure S-2.B and we can note that their averaged values in the visible wavelength range (380nm-700nm) are $n_{cuticule}$ = 1.63 and $k_{cuticule}$ = 0.04; these mean values are consistent with the literature mentioned above. These measured real and imaginary index values versus wavelength have been used in all our simulations.

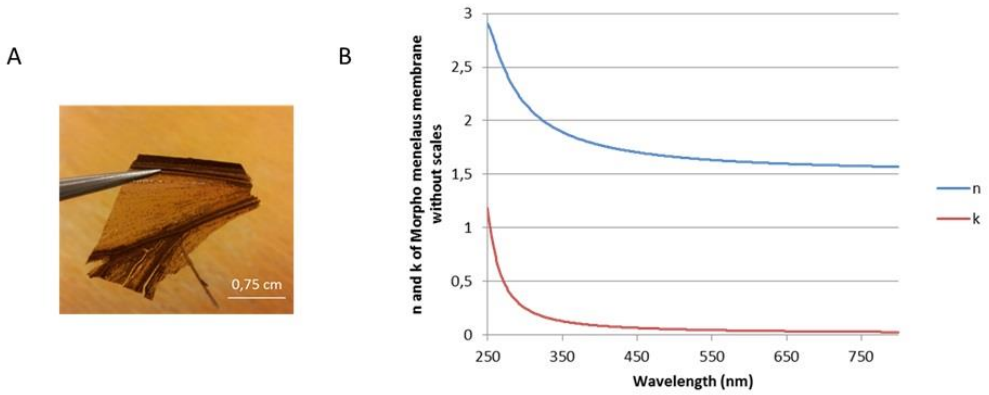

Figure S-2. A) Membrane of a *Morpho menelaus* wing after removing scales; B) n and k measured values of the membrane shown in A that are used for our ridge models.

Acknowledgments

This work was supported by the Cluster of Excellence MATISSE.

Disclosures

The authors declare no conflicts of interest.

References

1. A. Parker, "A vision for natural photonics," Philos. Transactions Royal Soc. A **362**, 2709–2720 (2004).
2. G.S. Smith, "Structural color of *Morpho* butterflies," Am. J. Phys. **77**, 1010–1019 (2009).
3. M.F. Land, "The physics and biology of animal reflectors," Prog. biophysics molecular biology **24**, 75–106 (1972).
4. A. Saito, Y. Miyamura, Y. Ishikawa, J. Murase, M. Akai-Kasaya, Y. Kuwahara, "Reproduction, mass-production, and control of the *Morpho*-butterfly's blue," Proc. SPIE **7205**, 720506-1–720506-9 (2009).
5. M. A. Giraldo, S. Yoshioka, C. Liu and D. G. Stavenga, "Coloration mechanisms and phylogeny of Morpho butterflies" Journal of Experimental Biology (2016) 219, 3936-3944 doi:10.1242/jeb.148726
6. M. A. Giraldo, S. Yoshioka & D. G. Stavenga, "Far field scattering pattern of differently structured butterfly scales", *Journal of Comparative Physiology A* **volume 194**, pages201–207(2008)
7. S. Berthier, E. Charron, J. Boulenguez "Structures and optical properties of the wings of Morphidae.", *Insect Sciences* **13** (2006) 145-157
8. V.Debat, S.Berthier, P.Blandin, N.Chazot, M.Elias, D.Gomez, V.Llaurens, "Why are the Morpho blue" in "Biodiversity and evolution", ISTE Press – Elsevier (2018).https://doi.org/10.1016/B978-1-78548-277-9.50009-7
9. J. Boulenguez, S. Berthier, F. Leroy, "Multiple scaled disorder in the photonic structure of *Morpho rhetenor* butterfly," Appl. Phys. A **106**, 1005–1011 (2012).
10. B. Song, S.C. Eom, J.H. Shin, "Disorder and broad-angle iridescence from *Morpho*-inspired structures," Opt. Express **22**, 19386–19400 (2014).
11. S. Yoshioka, S. Kinoshita, "Structural or pigmentary? Origin of the distinctive white stripe on the blue wing of a *Morpho* butterfly," Proc. Royal Soc. B **273**, 129–134 (2006).
12. R.A. Potyrailo, R.K. Bonam, J.G. Hartley, T.A. Starkey, P. Vukusic, M. Vasudev, T. Bunning, R.R. Naik, Z. Tang, M.A. Palacios, M. Larsen, L.A. Le Tarte, J.C. Grande, S. Zhong, T. Deng, "Towards utperforming conventional sensor arrays with fabricated individual photonic vapour sensors inspired by *Morpho* butterflies," Nat. Commun. **6**, 7959 (2015).
13. Watanabe, T. Hoshino, K. Kanda, Y. Haruyama, S. Matsui, "Brilliant Blue Observation from a *Morpho*-Butterfly-Scale Quasi-Structure," Jpn. J. Appl. Phys. **44**, L48–L50 (2004).
14. J. Huang, X. Wang, Z.L. Wang, "Controlled Replication of Butterfly Wings for Achieving Tunable Photonic Properties," Nano Lett. **6** (10), 2325–2331 (2006).
15. D.P. Gaillot, O. Deparis, V. Welch, B.K. Wagner, J.-P. Vigneron, C.J. Summers, "Composite organic-inorganic butterfly scales: Production of photonic structures with atomic layer deposition," Phys. Rev. E **78**, 031922 (2008).
16. W. Zhang, D. Zhang, T. Fan, J. Ding, Q. Guo, H. Ogawa, "Morphosynthesis of hierarchical ZnO replica using . butterfly wing scales as templates," Microporous Mesoporous Mater. **92**, 227–233 (2006).
17. W. Zhang, D. Zhang, T. Fan, J. Ding, J. Gu, Q. Guo, H. Ogawa, "Biomimetic zinc oxide replica with structural color using butterfly (*Ideopsis similis*) wings as templates," Bioinspiration Biomimetics **1**, 89–95 (2006).
18. Y. Chen, J. Gu, S. Zhu, T. Fan, D. Zhang, Q. Guo, "Iridescent large-area ZrO2 photonic crystals using butterfly as templates," Appl. Phys. Lett. **94**, 053901 (2009).
19. S. Zhu, D. Zhang, Z. Chen, J. Gu, W. Li, H. Jiang, G. Zhou, "A simple and effective approach towards biomimetic replication of photonic structures from butterfly wings," Nanotechnology **20**, 315303 (2009).
20. M. Thomé, L. Nicole, S. Berthier, "Multiscale replication of iridescent butterfly wings," Mater. Today: Proc. **1**, 221–224 (2014).
21. M. Thomé, L. Nicole, S. Berthier, "Sol-gel molding: a new observation method of multiscaled structures," Mater. Today: Proc. **4**, 5013–5022 (2017).
22. A. Mejdoubi, C. Andraud, S. Berthier, J. Lafait, J. Boulenguez, E. Richalot, "Finite Element modeling of the radiative properties of *Morpho* butterfly wing scales," Phys. Rev. E **87**, 022705 (2013).
23. R.H. Siddique, S. Diewald, J. Leuthold, H. Hölscher, "Theoretical and experimental analysis of the structural pattern responsible for the iridescence of *Morpho* butterflies," Opt. Express **21**, 14351–14361 (2013).
24. R.T. Lee, G.S. Smith, "Detailed electromagnetic simulation for the structural color of butterfly wings," Appl. Opt. **48**, 4177–4190 (2009).
25. L. Plattner, "Optical properties of the scales of *Morpho rhetenor* butterflies: theoretical and experimental investigation of the back-scattering of light in the visible spectrum," J. Royal Soc. interface **1**, 49–59 (2004).
26. M.-M. Huangfu, Y.-J. Liu, X. Xie, Y. Zhang, H.-W. Yang, "Research on surface lossy electromagnetic scattering of the scales of *Morpho rhetenor* butterflies," Optik **127** (10), 4418–4421 (2016).

27. D.Zhu, S. Kinoshita, D. Cai, and J.B. Cole, "Investigation of structural colors in Morpho butterflies using the nonstandard-finite-difference time-domain method: Effects of alternately stacked shelves and ridge density". Physical Review E80, 051924 (2009)
28. G. Liao, H. Zuo, Y. Cao, T. Shi, "Optical properties of the micro/nanostuctures of *Morpho* butterfly wing scales," Sci. China Ser. E: Technol. Sci. **53** (1), 175–181 (2010).
29. H.M. Kim, S.H. Kim, G.J. Lee, K. Kim, Y.M. Song, "Parametric studies on artificial *Morpho* butterfly wingscales for optical device applications," J. Nanomater. **16** (1), 368–374 (2015).
30. B. Gralak, G. Tayeb, S. Enoch, "*Morpho* butterflies wings color modeled with lamellar grating theory," Opt. Express **9**, 567–578 (2001).
31. E.J. Denton, M.F. Land, "Optical properties of the lamellae causing interference colours in animal reflectors," J. Physiol. **191**, 23–24 (1967).
32. P. Vukusic, J.R. Sambles, C.R. Lawrence, R.J. Wootton, "Quantified interference and diffraction in single Morpho butterfly scales," Proc. The Royal Soc. B **266**, 1403–1411 (1999).
33. S. Berthier, E. Charron, A. Da Silva, "Determination of the cuticle index of the scales of the iridescent butterfly *Morpho menelaus*," Opt. Commun. **228**, 349–356 (2003).
34. H. Arwin, T. Berlind, B. Johs, K. Järrendahl, "Cuticle structure of the scarab beetle *Cetonia aurata* analyzed by regression analysis of Mueller-matrix ellipsometric data," Opt. Express **21**, 22645–22656 (2013).
35. H.L. Leertouwer, B.D. Wilts, D.G. Stavenga, "Refractive index and dispersion of butterfly chitin and bird keratin measured by polarizing interference microscopy," Opt. Express **19**, 24061–24066 (2011).
36. R. Nishiyama, S. Yoshioka, "Detailed analysis of photonic structure in the wing scale of Rajah Brooke's birdwing butterfly" Optics express, 28(11) 2020, 16782-16794.
37. B. D. Wilts, M. A. Giraldo, D. G. Stavenga, "Unique wing scale photonics of male Rajah Brooke's birdwing butterflies", Wilts et al. Frontiers in Zoology (2016) 13:36
38. S. Berthier "Photonique des Morphos," Springer-Verlag (2010).
39. S. Berthier, "Thermoregulation and spectral selectivity of the tropical butterfly *Prepona meander* : a remarkable example of temperature auto-regulation." *Appl. Phys. A***80** (2003) 1397
40. Harry K. Clench, "Behavioural Thermoregulation in Butterflies https"://doi.org/10.2307/1935649
41. Tsai, C., Childers, R.A., Nan Shi, N. *et al.* Physical and behavioral adaptations to prevent overheating of the living wings of butterflies. *Nat Commun* **11,** 551 (2020). https://doi.org/10.1038/s41467-020-14408-8
42. P. Grasse. Traité de Zoologie, Insectes : Tête, ailes et vol. tome 8, fascicule 1, Insectes supérieurs, tome 10, Fascicule 1. Masson & Cie. Paris (1973).
43. https://sci-soft.com/product/film-wizard/